NOAA Technical Memorandum ERL PMEL-112

IMPLEMENTATION AND TESTING OF THE METHOD OF SPLITTING TSUNAMI (MOST) MODEL

V.V. Titov
F.I. Gonzalez

Pacific Marine Environmental Laboratory
7600 Sand Point Way NE
Seattle, WA 98115-0070

November 1997

Contribution No. 1927 from NOAA/Pacific Marine Environmental Laboratory

CONTENTS

Figures

Implementation and Testing of the Method of Splitting Tsunami (MOST) Model

V.V. Titov and F.I. Gonzalez

Abstract. A suite of numerical simulation codes, known collectively as the MOST (Method of Splitting Tsunami) model, has been implemented and tested. The MOST model is capable of simulating three processes of tsunami evolution, i.e., generation by an earthquake, transoceanic propagation, and inundation of dry land. Generation and propagation capabilities were tested against deep ocean bottom pressure recorder (BPR) data collected by PMEL during the 1996 Andreanov tsunami; inundation computations were compared with field measurements of maximum runup on Okushiri Island collected shortly after the 1993 Hokkaido-Nansei-Oki tsunami. Computed estimates agreed well with observations, indicating that the MOST model will be a valuable tool in the development of tsunami forecasting and hazard mitigation tools.

1. Introduction

The MOST model has been developed as part of the Early Detection and Forecast of Tsunami (EDFT) project, funded by the Defense Advanced Research Projects Agency (DARPA). This model is a suite of integrated numerical codes capable of simulating tsunami generation by a source near Alaska, its propagation across the Pacific Ocean, and its subsequent runup onto the Hawaiian shoreline; it will be used to develop tsunami hazard mitigation tools for the Pacific Disaster Center (PDC).

Simulation of the generation process in the MOST model is based on elastic deformation theory (Gusiakov, 1978; Okada, 1985), as described in Titov (1997), and the method of computing inundation is a derivative of the VTCS model (Titov, 1997; Titov and Synolakis, 1997, 1996, 1995). The global propagation code was developed specifically for the EDFT project. This report describes the MOST model, its implementation at the Center for Tsunami Mapping Inundation Efforts (TIME), and the results of preliminary testing.

2. The MOST Model

The evolution of earthquake-generated tsunami waves has three distinctive stages: generation, propagation, and runup. The MOST numerical model computes all three stages, providing a complete tsunami simulation capability.

2.1 Generation

The generation stage of tsunami evolution includes the formation of the initial disturbance of the ocean surface due to the earthquake-triggered deformation of the seafloor. This initial water-surface disturbance evolves into a long gravity wave radiating from the earthquake source. Modeling

of the initial stage of tsunami generation is therefore closely linked to studies of earthquake source mechanisms.

The tsunami generation process is based on a fault plane model of the earthquake source (Gusiakov, 1978; Okada, 1985) which assumes an incompressible liquid layer on an underlying elastic halfspace to characterize the ocean and the Earth's crust. The implementation of this elastic fault plane model (Titov, 1997) utilizes a formula for static sea-floor deformation to calculate the initial conditions required for subsequent computations of tsunami propagation and inundation.

2.2   Propagation

A tsunami can propagate long distances before it strikes a shoreline hundreds or thousands of kilometers from the earthquake source. To accurately model tsunami propagation over such large distances, the Earth's curvature should be taken into account. Other factors, such as Coriolis forces and dispersion, may also be important.

Dispersion changes the wave shape due to slightly different propagation speeds of waves with different frequencies. This effect can be taken into account even without the explicit use of dispersive terms in the governing equations; Shuto (1991) suggested that this process could be simulated by exploiting the numerical dispersion inherent in finite-difference algorithms. This method accounts for dispersive effects, but allows the use of non-dispersive linear or non-linear equations for wave propagation modeling. The MOST propagation model uses a numerical dispersion scheme and the non-linear shallow-water wave equations in spherical coordinates, with Coriolis terms (Murty, 1984):

$$h_t + \frac{(uh)_\lambda + (vh\cos\phi)_\phi}{R\cos\phi} = 0$$

$$u_t + \frac{uu_\lambda}{R\cos\phi} + \frac{vu_\phi}{R} + \frac{gh_\lambda}{R\cos\phi} = \frac{gd_\lambda}{R\cos\phi} + fv$$

$$v_t + \frac{uv_\lambda}{R\cos\phi} + \frac{vv_\phi}{R} + \frac{gh_\phi}{R} = \frac{gd_\phi}{R} - fu,$$

where λ is longitude, ϕ is latitude, $h = h(\lambda, \phi, t) + d(\lambda, \phi, t)$, $h(\lambda, \phi, t)$ is the amplitude, $d(\lambda, \phi, t)$ is the undisturbed water depth, $u(\lambda, \phi, t)$, $v(\lambda, \phi, t)$ are the depth-averaged velocities in the longitude and latitude directions, respectively, g is the gravity acceleration, f is the Coriolis parameter ($f = 2\omega\sin\phi$), and R is the Earth radius. In the MOST model, these equations are solved numerically using a splitting method similar to that described by Titov (1997).

2.3   Testing of Generation and Propagation

The June 10, 1996 Andreanov tsunami was simulated as a preliminary test of the global propagation model, using several deep-ocean BPR records from the Andreanov database for

comparison with the computed time series. A simple, single-fault mechanism was assumed for the earthquake source. The Harvard solution, derived by inverting seismic data, provided estimates of the moment magnitude (7.3×10^{20} Nm), strike ($260°$), dip ($20°$), and slip ($108°$). The aftershock distribution was used to estimate the fault length (140 km) and width (70 km). Finally, the relationship ($M = \mu UA$) between moment magnitude, M, the shear modulus, μ ($= 4.5 \times 10^{20}$ N/m^2), the average slip, U, and the fault area, A, (140×70 km^2) was used to estimate the magnitude of the slip (2 m). These fault-plane parameters were used in the elastic earthquake model to compute the static vertical sea-floor displacement; an identical displacement of the sea surface was then used as the initial condition for subsequent tsunami propagation computations.

Figure 1 shows the epicenter of the Andreanov earthquake and the locations of the deep-ocean BPRs. Figure 2 provides details of the shape and amplitude of the static ocean bottom displacement computed by the generation code; it is this pattern that was used as the initial sea surface elevation for subsequent tsunami computations. The MOST model grid domain for simulation of tsunami propagation in the North Pacific extended from 15°N to 65°N and from 180°W to 120°W. Global bathymetry data with horizontal resolution of 4 minutes were used for the computation (Smith and Sandwell, 1994).

Figure 3 provides a comparison of the computed waveforms with those measured at the deep-ocean BPR locations. Although the maximum tsunami wave amplitudes are less than 10 mm, the waveforms are well defined and the time series comparisons bring to light a number of interesting aspects of the physical phenomena that deserve comment. (1) There is good correlation between the computed and measured time series for the first two long-period (>1 hr) waves that constitute the first 2½ hours of the records. (2) Preceding the arrival of the tsunami waves, other long-period oscillations are evident in the BPR records, suggesting that some of the long-period energy seen after tsunami arrival is also non-tsunami. This is most clearly seen in the comparison plots for stations AK70 and AK71, the two northernmost BPR locations; in particular, the measured low-frequency peak between the first and second tsunami wave maxima is probably non-tsunami. (3) There is also a north-to-south decrease in the amplitude of this non-tsunami low frequency energy (Figs. 1 and 2); this suggests that the source of this energy may be interactions with the shelf and trench, whose influence would decrease with distance. (4) Higher frequency energy is superimposed on both the computed time series after tsunami arrival and over the entire length of the BPR records; the measured and computed high-frequency oscillations are of similar amplitude (1–3 mm) and period (6–12 min). This suggests that at least some of the high-frequency energy is geophysical and not just instrumental noise, and that this energy may be tsunamigenic in origin. It is also a strong indication of deep ocean BPR sensitivity; these systems are probably able to detect tsunami signals as small as only a few millimeters. (5) The period of the first (positive) half-cycle of the initial tsunami wave decreases from north to south. This is consistent with the strike of 260° for the earthquake fault plane model; the resulting bottom deformation is characterized by a dipole of two approximately elliptical lobes, negative to the north and positive to the south, oriented with long axes in a generally east-west
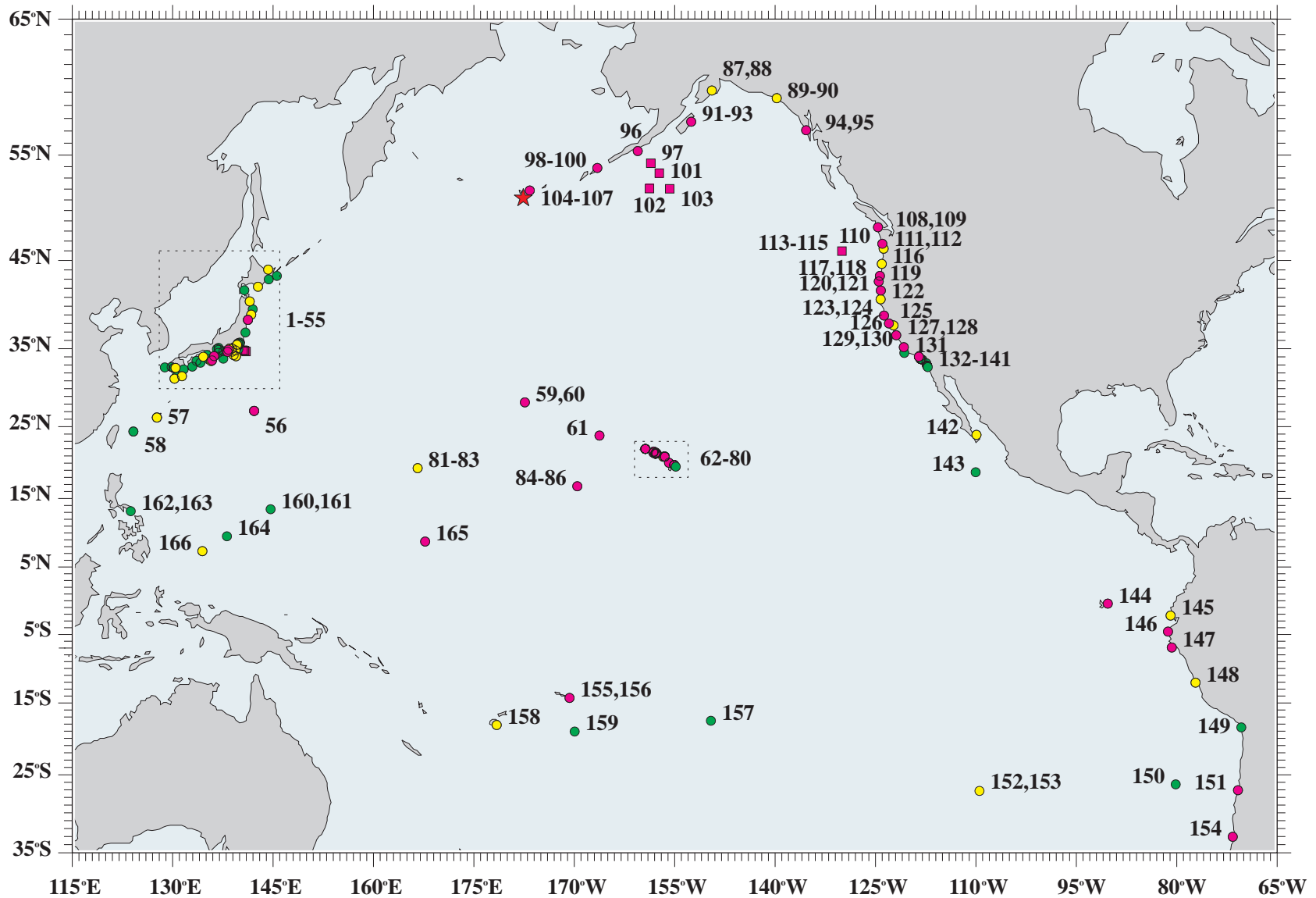
Fig. 1. Map showing the epicenter of the Andreanov earthquake (star) and all tsunami stations used in the database. Stations 97, 101–103, 113–115 are the deep ocean BPRs used for comparison with the MOST propagation model.
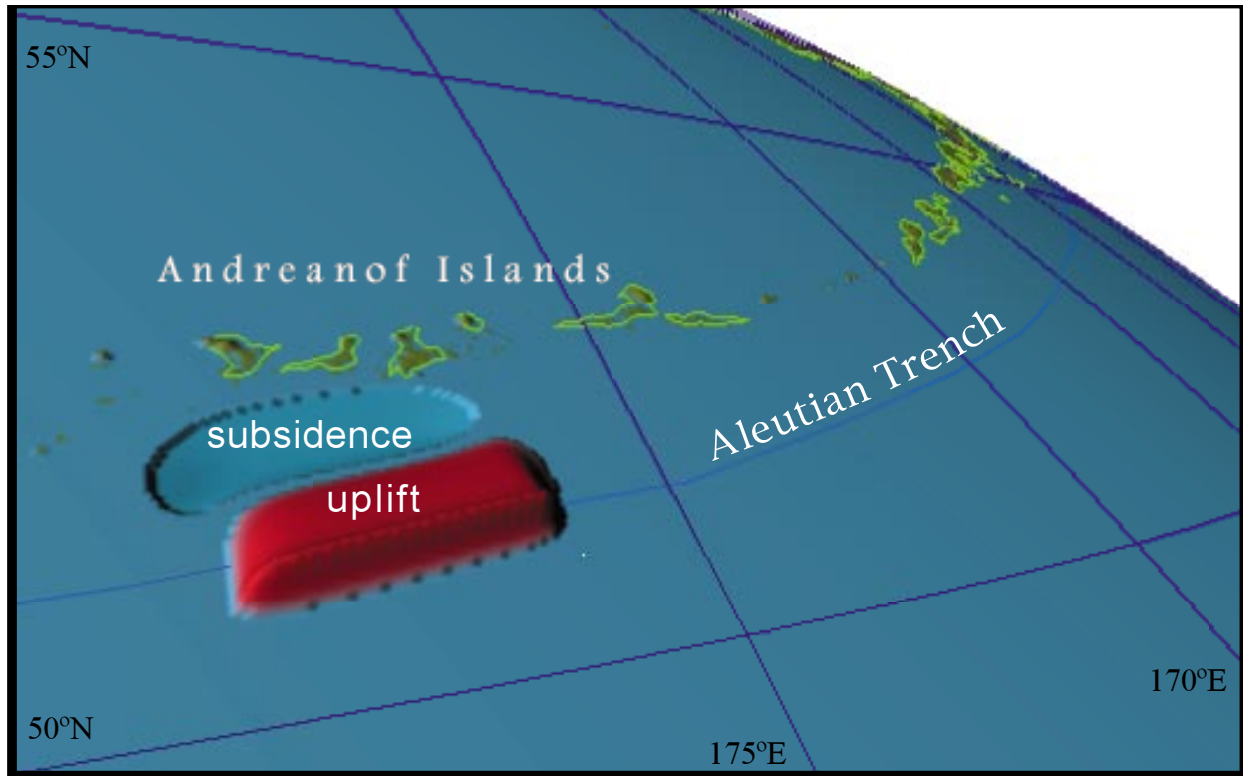
Fig. 2. Ocean bottom deformation pattern corresponding to the fault plane parameter estimates discussed in the text. The initial conditions for the subsequent propagation simulation assumed the same pattern of instantaneous sea level displacement.

direction. The wave period of energy generated by such a source will be a maximum at stations oriented along the long axis, and will decrease to a minimum at stations oriented along the short axis. (6) The second (negative) half-cycle that follows the first is of lower amplitude than the first (positive) half-cycle. This is also consistent with the relative sizes of the positive and negative lobes of the dipole source; the northern, negative, lobe is of significantly lower amplitude than the southern, positive, lobe. An exception is seen at Station WC67; this may be due to local low-frequency energy which destructively interfered with the second half-cycle.

2.4   Inundation

Runup of a tsunami onto dry land is probably the most underdeveloped part of any tsunami simulation model, primarily because of a serious lack of two major types of data—high quality field measurements for testing of the models, and fine-resolution bathymetry/topography data.

The first major obstacle to improving simulations of the inundation process, i.e., the lack of high-quality experimental and field measurements of runup, has been especially severe. Recently, this problem has been somewhat alleviated by a series of large-scale runup experiments conducted at the Coastal Engineering Research Center (CERC) of the U.S. Corps of Engineers (Briggs *et al.*,
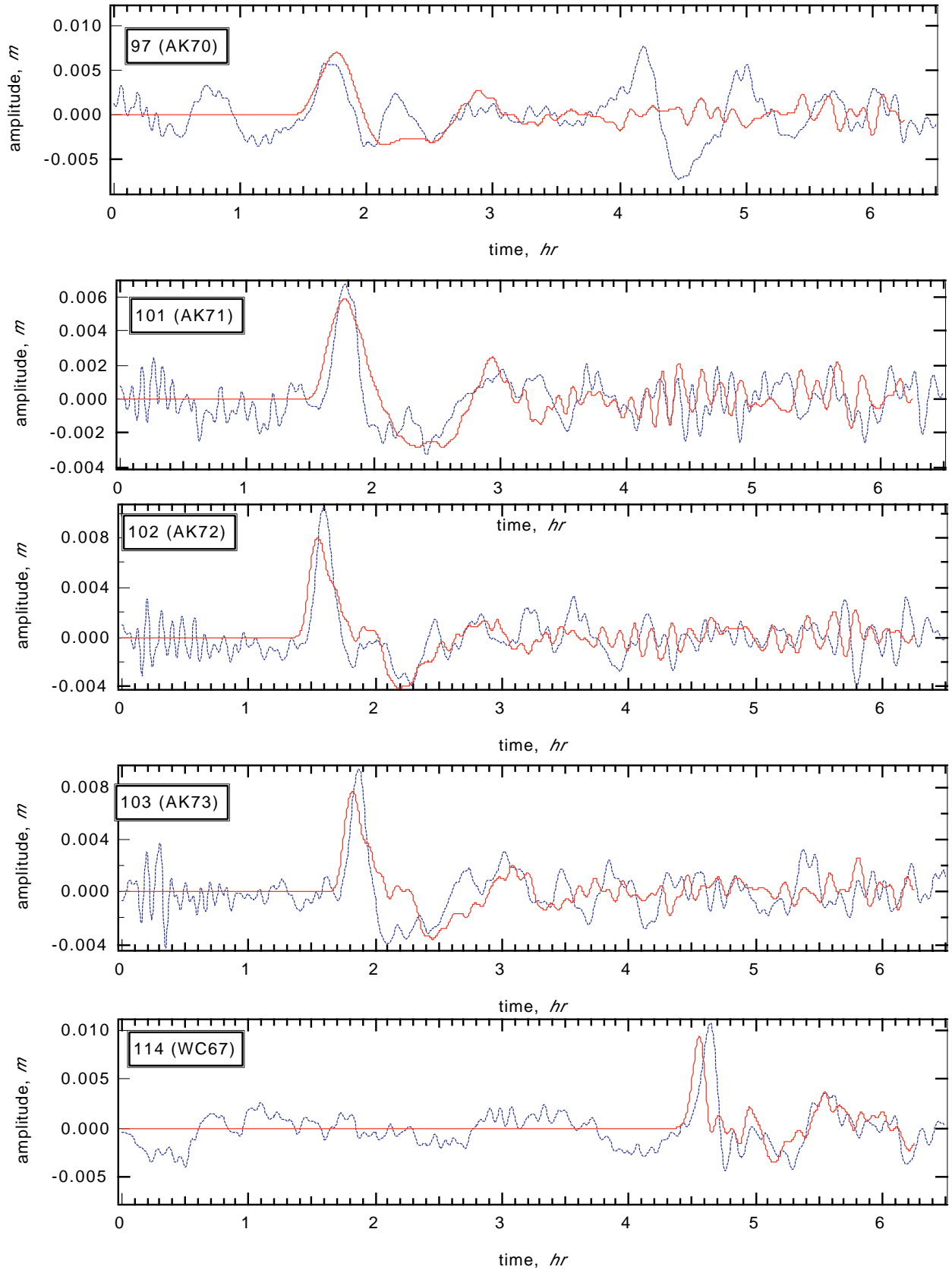
Fig. 3. Comparison between computed (continuous line) and BPR (dotted line) waveforms. Plot annotation refers to the BPR record number (see Fig. 1) and the Station Identification number (in parentheses).
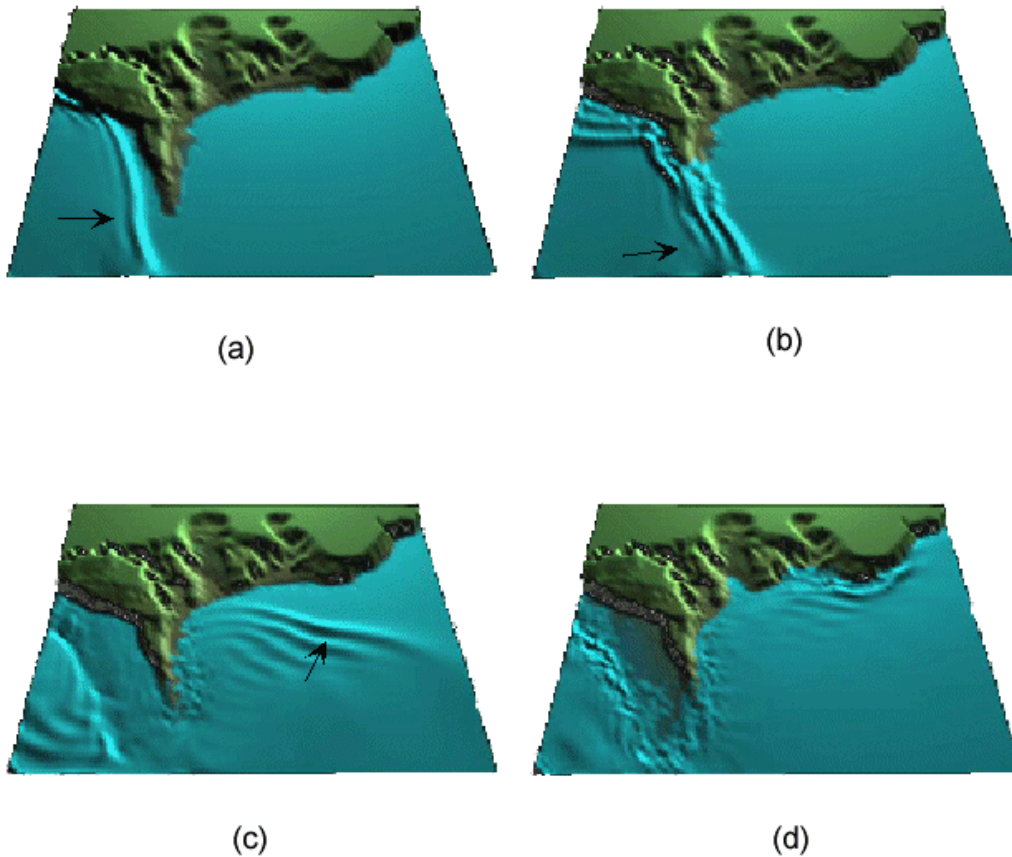
Fig. 4. Bird's-eye views of the computed tsunami waves overflowing the Aonae peninsula at (a) 5, (b) 6, (c) 8, and (d) 12 minutes after the earthquake main shock. The arrow indicates the direction of propagation of the wave front.

1995) and by several post-tsunami surveys which provided high quality field data (Yeh *et al.*, 1993; Synolakis *et al.*, 1995; Imamura *et al.*, 1995; Yeh *et al.*, 1995; Borrero *et al.*, 1997).

The second serious obstacle to accurate inundation model simulations is the requirement for high-resolution bathymetry and topography data in critical near-shore areas; in most cases, 10–50 m horizontal resolution of gridded bathymetry and topography data are essential. Such high-resolution data are not easily obtained; in particular, none are presently available for Hawaiian coastlines of interest.

Fortunately, however, high-resolution bathymetry and topography data for Okushiri Island, Japan, were made available by Tohoku University; this allowed the MOST model inundation computations to be tested against field data collected shortly after the July 12, 1993 Hokkaido-Nansei-Oki tsunami.

Figure 4 illustrates the inundation of the Aonae peninsula computed with the MOST inundation model. The figure provides four snapshots of bird's-eye views of the Aonae peninsula
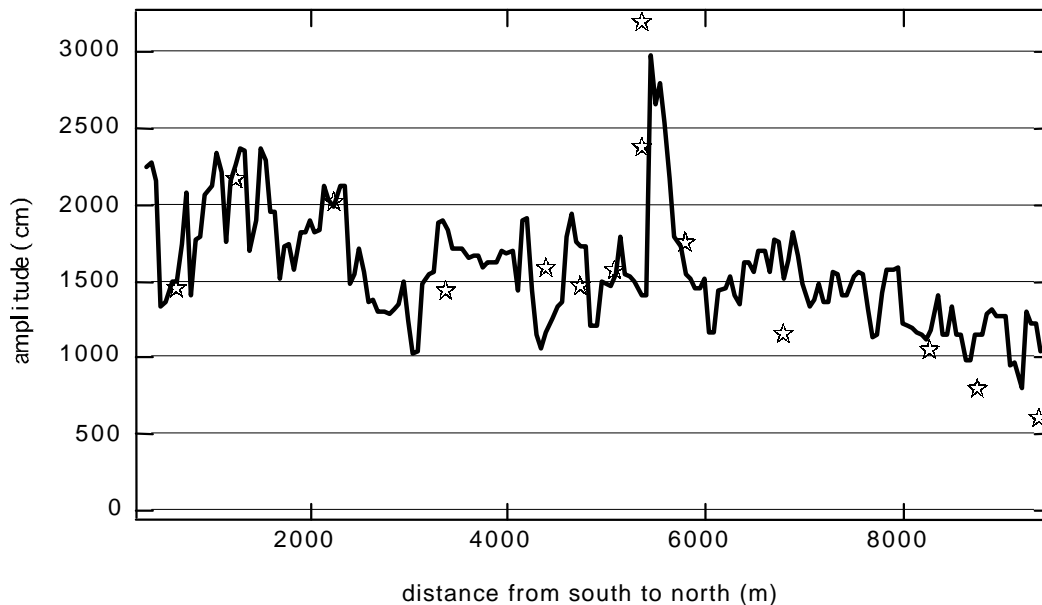
Fig. 5. Comparison of computed (solid line) and measured (stars) maximum runup values along the west coast of Okushiri island.

during the tsunami runup. An important result of this simulation, consistent with rough field estimates, is the very high maximum water velocity computed—more than 18 m/s, i.e., more than 40 knots (Titov, 1997). It is believed that this tremendous current, made much more destructive by large floating objects in the water (automobiles, small boats, logs, etc.) that became battering rams, was the principal mechanism responsible for the disastrous damage and loss of more than 200 lives.

Figure 5 provides a comparison of computed and measured maximum inundation values along the west coast of Okushiri. Agreement is good, suggesting that, where adequate bathymetric and topographic data are available, the MOST model inundation computations are sufficiently accurate to develop useful hazard mitigation tools and guidance products such as inundation maps.

3. Implementation

Development and preliminary testing of the MOST model was conducted at PMEL. On completion of this development phase, an agreement was reached with DARPA to transfer the model to the Center for Tsunami Inundation Mapping Efforts (TIME), the inundation mapping component of the National Tsunami Hazard Mitigation Plan (Tsunami Hazard Mitigation Federal/State Working Group, 1996).

The MOST model was transferred to the TIME Center and implemented on a Silicon Graphics, Inc. (SGI) Octane R10000 dual-processor workstation with Explorer visualization software. This computer platform is identical to the computer system at PMEL on which the model was originally developed and implemented, ensuring that the TIME Center implementation of the MOST model

has the same capabilities summarized in this report. All three components of the MOST model—the generation, propagation and runup codes—were installed, and preliminary tests of all components were performed to ensure functionality. TIME personnel continue to be trained in the use of the MOST model, and we anticipate that strong, mutually beneficial relationships will develop between the TIME Center modeling activity, the PDC, and the associated Maui High Performance Computing Center (MHPCC).

4. Summary and Conclusion

A suite of tsunami generation, propagation, and inundation numerical simulation codes, known collectively as the Method of Splitting Tsunami (MOST) model, has been developed, implemented, and tested on SGI workstations at PMEL and the TIME Center. Generation and propagation capabilities were compared with deep-ocean data collected by PMEL during the June 10, 1996 Andreanov tsunami, and inundation computations were checked against runup measurements acquired on Okushiri Island shortly after the July 12, 1993 Hokkaido-Nansei-Oki tsunami. Model results compared well with field measurements of both propagation and inundation. The MOST model was able to reproduce the dominant deep-ocean waveform from a distant tsunami with considerable accuracy, and the inundation computations resulted in runup distributions that were very similar to the actual observations. We view these results as encouraging and as a positive indication of the potential utility of the MOST model. In particular, we conclude that the MOST model will be of great value in the development of useful tsunami hazard mitigation and forecasting tools.

5. Future Plans

As part of an anticipated FY1998–FY2000 modeling project focused on developing tsunami hazard mitigation and forecast tools for the PDC (Bernard *et al.*, 1997), the MOST model codes will be parallelized and implemented on the SP supercomputer at the MHPCC. This supercomputer implementation will allow the efficient computation of many scenarios, and the capability will be used to perform multiple-run sensitivity studies of two closely related, but separable, processes—offshore wave dependence on distant earthquake magnitude and position, and site-specific inundation dependence on offshore wave characteristics. The results will be organized into an electronic database, and associated software will be developed for analysis and visualization of this database, including the assimilation of real-time data streams; the goal is to provide guidance for forecasting and hazard assessment during an actual event.

In the more distant future, it may become technically feasible and scientifically justified to execute real-time model runs for guidance, as an actual event unfolds. As currently implemented on an SGI Octane workstation, the computation of 6.5 hours of tsunami propagation takes about 1 hour; as the model is implemented on even faster, parallel architecture platforms, such as the MHPCC supercomputer, the computing/real time ratio will drop dramatically, perhaps by a factor of 10–100.

But an operational real-time model forecasting capability must await improved and more detailed characterization of earthquakes in real time, and verification that the real-time tsunami model computations are sufficiently robust to be used in an operational, real-time mode. Unfortunately, the existing state of the art in tsunami modeling still requires considerable quality control, judgment, and iterative, exploratory computations before a scenario is assumed reliable. This is why the creation of a database of pre-computed scenarios that have been carefully analyzed and interpreted by a knowledgeable and experience tsunami modeler is an essential first step in the development of a reliable and robust tsunami forecasting and hazard assessment capability.

6.   Acknowledgments

7.   References

Borrero, J., M. Ortiz, V. Titov, and C.E. Synolakis (1997): Field survey of Mexican tsunami produces new data, unusual photos. *Eos Trans. AGU, 78*(8), 85, 87–88.

Briggs, M.J., C.E. Synolakis, G.S. Harkins, and D.R. Green (1995): Laboratory experiments of tsunami runup on circular island. *Pure Appl. Geophys., 144*(3/4), 569–593.

Bernard, E.N, F.I. Gonzalez, and V.V. Titov (1997): Pacific Disaster Center Tsunami Forecasting Capabilities via the Tsunami Community Modeling Facility. A Proposal to the Office of the Assistant Deputy Under-Secretary of Defense for Space Integration, August, 1997.

Gusiakov, V.K. (1978): Static displacement on the surface of an elastic space. Ill-posed problems of mathematical physics and interpretation of geophysical data, Novosibirsk, VC SOAN SSSR, 23–51 (in Russian).

Imamura, F., C.E. Synolakis, E. Gica, V. Titov, E. Listanco, and H.G. Lee (1995): Field survey of the 1994 Mindoro Island, Philippines tsunami. *Pure Appl. Geophys., 144*, 875–890.

Murty, T.S. (1984): Storm surges–meteorological ocean tides. *Bull. 212, Fish. Res. Board,* Canada, Ottawa, 897 pp.

Okada, Y. (1985): Surface deformation due to shear and tensile faults in a half space. *Bull. Seism. Soc. Am., 75*, 1135–1154.

Shuto, N. (1991): Numerical simulation of tsunamis. In *Tsunami Hazard*, Bernard, E. (ed.), Kluwer Academic Publishers, Dordrecht, The Netherlands, 171–191.

Smith, W.H.F., and D.T. Sandwell (1994): Bathymetric prediction from dense satellite altimetry and sparse shipboard bathymetry. *J. Geophys. Res., 99*, 21,803–21,824.

Synolakis, C.E., F. Imamura, S.Tinti, Y. Tsuji, H. Matsutomi, B. Cooke, and M. Usman (1995): The East Java tsunami of July 4, 1994. *Eos Trans. AGU, 76*(26), 257, 261–262.

Titov, V.V., and C.E. Synolakis (1997): Extreme inundation flows during the Hokkaido-Nansei-Oki tsunami. *Geophys. Res. Lett, 24*(11), 1315–1318.

Titov, V.V. (1997): Numerical modeling of long wave runup. Ph.D. thesis, University of Southern California, Los Angeles, California, 141 pp.

Titov, V.V., and C.E. Synolakis (1996): Numerical modeling of 3-D long wave runup using VTCS-3. In *Long Wave Runup Models*, P. Liu, H. Yeh, and C. Synolakis (eds.), World Scientific Publishing Co. Pte. Ltd., Singapore, 242–248.

Titov, V.V., and C.E. Synolakis (1995): Modeling of breaking and nonbreaking long wave evolution and runup using VTCS-2. *J. Waterways, Ports, Coastal and Ocean Engineering, 121*(6), 308–316.

Tsunami Hazard Mitigation Federal/State Working Group (1996): Tsunami Hazard Mitigation Implementation Plan, A Report to the Senate Appropriations Committee, 22 pp. plus Appendices (the URL is http://www.pmel.noaa.gov/tsunami-hazard/).

Yeh, H., F. Imamura, C.E. Synolakis, Y. Tsuji, P.L.-F. Liu, and S. Shi (1993): The Flores island tsunamis. *Eos Trans. AGU, 7*(33), 369, 371–373.

Yeh, H., V. Titov, V.K. Gusiakov, E. Pelinovsky, V. Khramushin, and V. Kaistrenko (1995): The 1994 Shikotan earthquake tsunami. *Pure Appl. Geophys., 144*(3/4), 569–593.